する上で非常に有用な手段であることが示された。

E. 結論

新規変異遺伝子と病態との関連を明らかにする有用な方法としてin vivo エレクトロポレーション法を用いた方法を確立した。

F. 健康危険情報

特になし

G. 研究発表

1. 論文発表

Shalaby S, Mitsuhashi H, Matsuda C, Minami N, Noguchi S, Nonaka I, Nishino I, Hayashi YK: Defective Myotilin Homodimerization Caused by a Novel Mutation in MYOT Exon 9 in the First Japanese Limb Girdle Muscular Dystrophy 1A Patient. J Neuropathol Exp Neurol. 68: 701-707, 2009

Park YE, Hayashi YK, Bonne G, Arimura T, Noguchi S, Nonaka I, Nishino I: Autophagic degradation of nuclear components in mammalian cells. Autophagy. 5: 795-804, 2009

Tominaga K, Hayashi YK, Goto K, Minami N, Noguchi S, Nonaka I, Miki T, Nishino I: Congenital myotonic dystrophy can show congenital fiber type disproportion pathology. Acta Neuropathol. 119: 481-486, 2010

2. 学会発表

三橋里美, Shalaby S, 後藤加奈子、埜中征哉, 野口 悟, 林由起子, 西野一三: 本邦zaspopathy 症例における臨床筋病理学的検討. 第50回日本神経学会総会, 仙台, 5. 21, 2009

三橋弘明, Shalaby S, 松田知栄, 南 成祐, 野口 悟, 埜中征哉, 林由起子, 西野一三: 肢帯型筋ジストロフィー1A型患者に見出されたmyotilinのホモダイマー形成異常. 第82回日本生化学会大会, 神戸, 10. 24, 2009

Hayashi YK, Goto K, Noguchi S, Nishino I: Screening the FHL1 mutation in Japanese patients with non-4q35 FSHD. 14th International Congress of the World Muscle Society (WMS), Geneva, Switzerland, 9.10, 2009

Shalaby S, Hayashi YK, Mitsuhashi H, Goto K, Nonaka I, Noguchi S, Nishino I: New variant of myofibrillar myopathy with CNS involvement. 14th International Congress of the World Muscle Society (WMS), Geneva, Switzerland, 9.11, 2009

Tominaga K, Hayashi YK, Goto K, Minami N, Noguchi S, Nonaka I, Nishino I: Congenital myotonic dystrophy in

patients diagnosed as congenital fiber type disproportion. 14th International Congress of the World Muscle Society (WMS), Geneva, Switzerland, 9.11, 2009

Park YE, Hayashi YK, Bonne G, Arimura T, Noguchi S, Nonaka I, Nishino I: Autophagic degradation of nuclear component in nuclear envelopathy. 14th International Congress of the World Muscle Society (WMS), Geneva, Switzerland, 9.11, 2009

Hayashi YK, Park YE, Bonne G, Arimura T, Noguchi S, Nonaka I, Nishino I: Autophagic degradation of nuclear components in mammalian cells. The 5th International Symposium on Autophagy: Molecular Mechanism, Cellular and Physiological Functions and Diseases, Ots, 9.28, 2009

H. 知的財産権の出願・登録状況

1. 特許取得

なし

2. 実用新案登録

なし

3. その他

なし

厚生労働科学研究費補助金（こころの健康科学研究事業）
分担研究報告書

サルコメア配列異常を主病変とする筋ジストロフィーの細胞生物学的解析に関する研究

研究分担者　松田　知栄　独立行政法人産業技術総合研究所　主任研究員

研究要旨　筋原線維性ミオパチー患者で見いだされた変異遺伝子産物の疾患との関連を明らかにするために、Z線関連タンパク質および結合タンパク質の変化について解析した。

A. 研究目的

筋原線維性ミオパチー（MFM）の原因遺伝子タンパク質の多くはZ線関連タンパク質であり、そのタンパク質相互連関が病態と深く関わっていると考えられる。そこで本研究では変異を同定し得たMFM患者骨格筋におけるZ線関連タンパク質の変化を検討した。

B. 研究方法

変異スクリーニングの結果、変異の見いだされた患者骨格筋について、免疫組織化学的、生化学的解析を行った。

（倫理面への配慮）

本研究において使用した全てのヒト検体は、いずれも疾患の確定診断のために病理学的、生化学的、免疫学的ならびに遺伝子レベルの解析が必要であり、かつ患者および家族もこれを希望し、患者および家族の了解を得た上で採取された組織（生検・剖検筋、皮膚、血球など）を用いて得られたものであり、かつ、国立精神・神経センター倫理委員会で承認された所定の承諾書を用いて、患者あるいはその親権者から遺伝子解析を含む研究使用に対する検体の使用許可（インフォームドコンセント）を得たものである。遺伝子解析に関しては「ヒトゲノム解析研究に関する共通指針」を遵守した上で、施行されたものである。これらの情報を使用するに当たっては、プライバシーを尊重し、匿名化した上で使用した。

C. 研究結果

我々の見いだした新規*MYOT*変異について酵母2ハイブリッド法を用いて、ミオティリンの二量体形成能およびαアクチニンとの結合性の低下を明らかにした(JNEN, 2009)。また*ZASP*変異例については他のZ線局在タンパク質の機能異常を明らかにした（論文投稿準備中）。

D. 考察

MFM 患者骨格筋では Z 線タンパク質の機能・局在異常が病態と深く関わっている可能性が示唆された。

E. 結論

MFM骨格筋を用いて、Z線タンパク質の相互連関及びその機能を明らかにしていく必要がある。

F. 健康危険情報

特になし

G. 研究発表

1. 論文発表

Shalaby S, Mitsuhashi H, Matsuda C, Minami N, Noguchi S, Nonaka I, Nishino I, Hayashi YK: Defective Myotilin Homodimerization Caused by a Novel Mutation in MYOT Exon 9 in the First Japanese Limb Girdle Muscular Dystrophy 1A Patient. J Neuropathol Exp Neurol. 68: 701-707, 2009

Hayashi YK, Matsuda C, Ogawa M, Goto K, Tominaga K, Mitsuhashi S, Park YE, Nonaka I, Hino-Fukuyo N, Haginoya K, Sugano H, Nishino I: Human PTRF mutations cause secondary deficiency of caveolins resulting in muscular dystrophy with generalized lipodystrophy. J Clin Invest. 119: 2623-2633, 2009

2. 学会発表

Matsuda C, Kameyama K, Nishino I, Hayashi YK: The association of dysferlin and affixin is regulated by calcium concentration. 14th International Congress of the World Muscle Society (WMS), Geneva, Switzerland, 9.10, 2009

H. 知的財産権の出願・登録状況

1. 特許取得

なし

2. 実用新案登録

なし

3. その他

なし

Ⅲ.　研究成果の刊行に関する一覧表

研究成果の刊行に関する一覧表

発表者氏名： 論文タイトル名. 発表誌名 巻号： ページ, 出版年
Shalaby S, Mitsuhashi H, Matsuda C, Minami N, Noguchi S, Nonaka I, Nishino I, Hayashi YK: Defective Myotilin Homodimerization Caused by a Novel Mutation in MYOT Exon 9 in the First Japanese Limb Girdle Muscular Dystrophy 1A Patient. *J Neuropathol Exp Neurol.* 68: 701-707, 2009
Park YE, Hayashi YK, Bonne G, Arimura T, Noguchi S, Nonaka I, Nishino I: Autophagic degradation of nuclear components in mammalian cells. *Autophagy.* 5: 795-804, 2009
Hayashi YK, Matsuda C, Ogawa M, Goto K, Tominaga K, Mitsuhashi S, Park YE, Nonaka I, Hino-Fukuyo N, Haginoya K, Sugano H, Nishino I: Human PTRF mutations cause secondary deficiency of caveolins resulting in muscular dystrophy with generalized lipodystrophy. *J Clin Invest.* 119: 2623-2633, 2009
Murakami T, Hayashi YK, Ogawa M, Noguchi S, Campbell KP, Togawa M, Inoue T, Oka A, Ohno K, Nonaka I, Nishino I: A novel POMT2 mutation causes mild congenital muscular dystrophy with normal brain MRI. *Brain Dev.* 31: 465-468, 2009
Tominaga K, Hayashi YK, Goto K, Minami N, Noguchi S, Nonaka I, Miki T, Nishino I: Congenital myotonic dystrophy can show congenital fiber type disproportion pathology. *Acta Neuropathol.* 119: 481-486, 2010

Ⅳ.　研究成果の刊行物・別刷

J Neuropathol Exp Neurol

Vol. 68, No. 6
June 2009
pp. 701–707

ORIGINAL ARTICLE

Defective Myotilin Homodimerization Caused by a Novel Mutation in *MYOT* Exon 9 in the First Japanese Limb Girdle Muscular Dystrophy 1A Patient

Sherine Shalaby, MD, Hiroaki Mitsuhashi, PhD, Chie Matsuda, PhD, Narihiro Minami, MS, Satoru Noguchi, PhD, Ikuya Nonaka, MD, PhD, Ichizo Nishino, MD, PhD, and Yukiko K. Hayashi, MD, PhD

Abstract

Myotilin is a muscle-specific Z disk protein. Several missense mutations in the myotilin gene (*MYOT*) have been identified in limb girdle muscular dystrophy (LGMD), myofibrillar myopathy, and distal myopathy patients. All previously reported pathogenic *MYOT* mutations have been identified only in Exon 2. We sequenced *MYOT* in 138 patients diagnosed as having LGMD, myofibrillar myopathy, or distal myopathy, and identified a novel *MYOT* mutation in Exon 9 encoding the second immunoglobulin-like domain in 1 patient with clinically typical LGMD. By light microscopy, there were scattered fibers with rimmed vacuoles and myofibrillary disorganization in the patient's muscle biopsy; accumulation of Z disk proteins was observed by immunohistochemistry. Immunoblot analysis demonstrated that the amount of myotilin monomer was increased in the patient muscle, but that the myotilin homodimeric band was decreased. Functional analysis of the myotilin mutation using a yeast 2-hybrid system revealed defective homodimerization of the mutant myotilin and decreased interaction between mutant myotilin and α-actinin. The homodimerization defect was further demonstrated by immunoprecipitation. This is the first *MYOT* mutation outside of Exon 2 in an LGMD type 1A patient and the first *MYOT* mutation identified in the Japanese population. This mutation in the second immunoglobulin-like domain impairs myotilin dimerization and alters the binding between myotilin and α-actinin, which is known to be important for actin bundling.

Key Words: Distal myopathy, Homodimer, Immunoglobulin-like domain, Limb girdle muscular dystrophy, Myofibrillar myopathy, Myotilin, Myotilinopathy.

INTRODUCTION

Myotilin (myofibrillar protein with titin-like immunoglobulin domains) is a sarcomeric Z disk protein encoded by the myotilin gene (*MYOT* or *TTID*) on chromosome 5q31 (1). Myotilin is composed of a unique serine-rich N-terminus and 2 immunoglobulin-like domains at the C-terminus (1–4). Myotilin forms a homodimer and interacts with α-actinin (1), actin (5), and filamin C (FLNC) (6, 7) at the Z disk through these immunoglobulin-like domains (Fig. 1A). Myotilin is highly expressed in skeletal muscle, cardiac muscle, and peripheral nerves (1). Myotilin plays a significant role in sarcomere assembly by acting together with α-actinin and FLNC to cross-link actin filaments into tightly packed bundles (1, 5, 8). The resulting structures support the integrity of the contracting muscle cell (6).

Missense mutations in *MYOT* cause myofibrillar myopathy (MFM) (9–11), limb girdle muscular dystrophy type 1A (LGMD1A) (11–13) and late-onset distal myopathy (14, 15). These myotilinopathies are usually associated with cardiac involvement and peripheral neuropathy and rarely with respiratory involvement. Currently, there are only 8 known *MYOT* mutations associated with myopathy (i.e. K36E, S39F, S55F, T57I, S60C, S60F, Q74K, and S95I) (8–11); all are located in Exon 2 encoding the serine-rich amino-terminal (Fig. 1A).

Here, we report the first Japanese LGMD1A patient associated with a novel mutation in the second immunoglobulin-like domain of myotilin and provide data suggesting the pathobiologic significance of this mutation.

MATERIALS AND METHODS

Clinical Materials

All clinical materials used in this study were obtained for diagnostic purposes with informed consent. We searched

From the Department of Neuromuscular Research, National Institute of Neuroscience, National Center of Neurology and Psychiatry, Kodaira, Tokyo (SS, HM, SN, IN, IN, YKH); Neuroscience Research Institute, AIST, Central 6, Tsukuba, Ibaraki (CM); and Department of Laboratory Medicine, National Center Hospital of Neurology and Psychiatry, National Center of Neurology and Psychiatry, Kodaira, Tokyo (NM), Japan.

Send correspondence and reprint requests to: Yukiko K. Hayashi, MD, PhD, Department of Neuromuscular Research, National Institute of Neuroscience, National Center of Neurology and Psychiatry, 4-1-1 Ogawahigashi-cho, Kodaira, Tokyo 187-8502, Japan; E-mail: hayasi_y@ncnp.go.jp

This study was supported by a grant-in-aid for scientific research and a grant-in-aid for exploratory research from the Japan Society for the Promotion of Science; by the Research on Psychiatric and Neurological Diseases and Mental Health of the Health Labour Sciences Research Grant and research grants (20B-12, 20B-13, 19A-4, and 19A-7) for Nervous and Mental Disorders from the Ministry of Health, Labour, and Welfare; by the Research on Health Sciences focusing on Drug Innovation from the Japanese Health Sciences Foundation; and by the Program for Promotion of Fundamental Studies in Health Sciences of the National Institute of Biomedical Innovation.

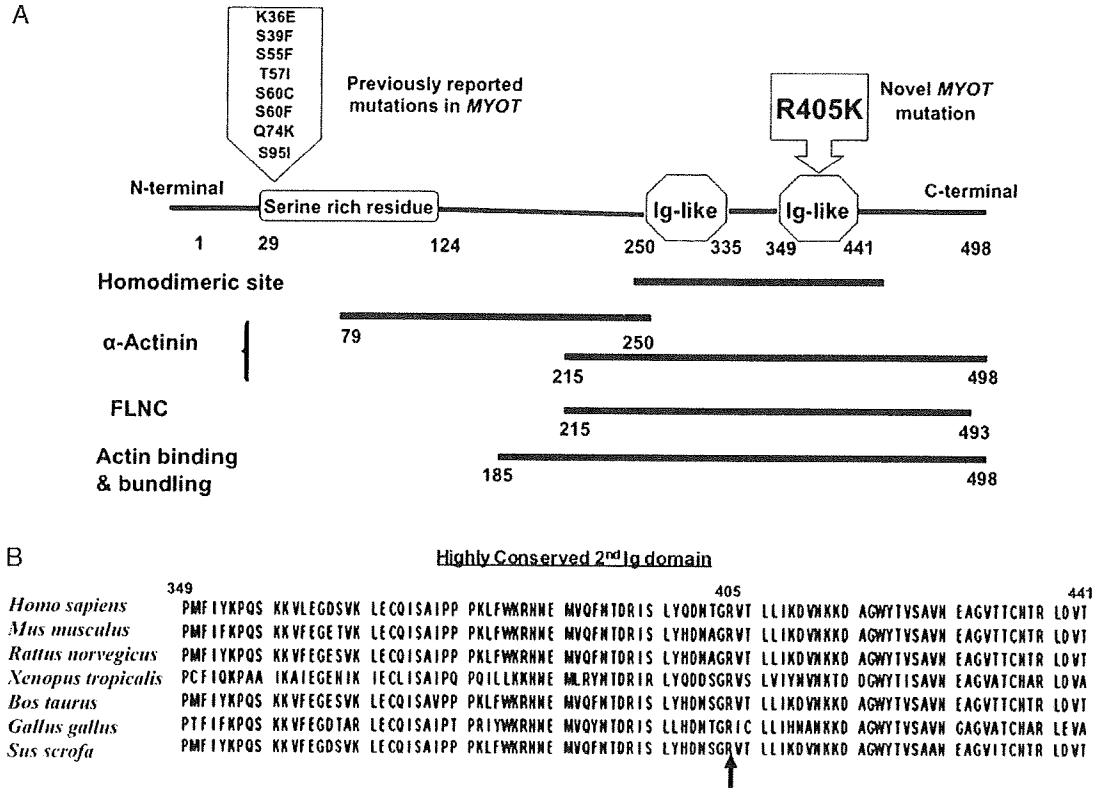

FIGURE 1. Myotilin structure, interacting partners, and reported mutations. **(A)** All previously reported mutations are located in the serine-rich domain; the novel mutation p.R405K identified in this study is located in the second immunoglobulin (Ig)-like domain of myotilin. Immunoglobulin domains of myotilin are regions of most myotilin interactions with other proteins. **(B)** The second Ig domain is highly conserved through species including the mutated residue p.R405 in the patient (arrow) (6–8). FLNC, filamin C.

for *MYOT* mutations in a total of 138 Japanese patients who had been diagnosed pathologically or clinically as MFM (n = 48), LGMD (n = 40), or distal myopathy (n = 50).

Genetic Analysis

Genomic DNA was isolated from peripheral lymphocytes or muscle specimens using standard techniques. Nine sets of primers were used to amplify genomic fragments of *MYOT*. All exons and their flanking intronic regions of *MYOT* were sequenced directly in all 138 patients using an ABI PRISM 3100 automated sequencer (PE Applied Biosystems, Foster City, CA). Nearly all of the patients with the different diagnoses were screened for *ZASP*, *DES*, and *CRYAB* mutations. Distal myopathy patients were also screened for *GNE* mutations. Primer sequences are available on request.

Histochemical Analysis

Biopsied muscle specimens were frozen in isopentane cooled in liquid nitrogen. Serial 10-μm cryosections were stained with hematoxylin and eosin, modified Gomori trichrome, nicotinamide adenine dinucleotide dehydrogenase-tetrazolium reductase, myosin ATPase phosphatase, and a battery of histochemical methods.

Immunohistochemistry and Immunoblotting

Immunohistochemistry and immunoblotting were performed as previously described (13, 16, 17). Antibodies used in this study are to: myotilin (kindly provided by Dr Carpén, University of Helsinki) (13), desmin (Abcam, Tokyo, Japan), Z-band alternatively spliced PDZ motif protein (ZASP) (Abcam), skeletal muscle actin (Nichirei, Tokyo, Japan), and αB-crystallin (Stressgen, Victoria, British Columbia, Canada).

Antibodies to dystrophin (Novocastra Laboratories, Newcastle upon Tyne, UK), sarcoglycans (Novocastra), α-dystroglycan (Upstate Biotechnology, Lake Placid, NY), dysferlin (Novocastra), caveolin-3 (BD Transduction Laboratories, Lexington, KY), calpain-3 (Novocastra), merosin (Chemicon International, Temecula, CA), collagen VI (ICN Biomedicals, Inc, Cleveland, OH), and emerin (Novocastra) were also used in the LGMD patients to exclude other diagnosable causes of muscular dystrophy.

Plasmid Construction

Total RNA was extracted from control human skeletal muscle using standard techniques; cDNA was synthesized by reverse transcription polymerase chain reaction with random hexamers. Full-length myotilin (wtMYOT), skeletal muscle

actin (ACTA1), α-actinin 2 (ACTN2), and the C-terminal portion (i.e. amino acids from 1967 to 2699) of FLNC were amplified using the following primers: MYOT, 5′-GGAATT CAGTAATAATTTGCCTTCA TCTTCCA-3′ and 5′-CGGGATCCACAAATCCATATACCCAGATTTCCT-3′; ACTA1, 5′-GGAATTCCAGAAACTAGACACAATGTG CGA-3′ and 5′-CGGGATCCAGTTGTTACAAAGAAAGT GACTGCG-3′; ACTN2, 5′-CCGGAATTCGCGGCCAC CATGGATTACAAGGATGACGACGACGATAAGAAC CAGATAGAGCCCGGCGT-3′ and 5′-CCGCTCGAGTCA CAGATCGCTCTCCCCGTA-3′; and FLNC, 5′-GGAATT CAAGATCACCGAGAGTGATCTGAGC-3′ and 5′-GTCGACCTCCTTGACAGTGTAGGTGACATTG-3′. The polymerase chain reaction products were cloned into the pGEM-T-easy vector (Promega, Madison, WI), and their sequences were confirmed. For expression in yeast, the cDNAs inserted in pGEM-T-easy were digested and ligated into the vectors pGBKT7 containing *GAL4* DNA-binding domain and pGADT7 containing *GAL4* activating domain (Takara Bio, Shiga, Japan). Mutant myotilin (mMYOT) (c.1214G>A) was generated by site-directed mutagenesis using the primers 5′-GATAACACTGGAAAAGTTACTTTACTG-3′ and 5′-CAGTAAAGTAACTTTTCCAGTGTTATC-3′.

Yeast 2-Hybrid Experiment

Yeast 2-hybrid (Y2H) assays aimed at testing specific interaction pairs were carried out as previously described (18–20). *Saccharomyces cerevisiae AH109* was double transformed with pGBKT7 constructs and pGADT7 constructs and selected on minimal medium lacking leucine and tryptophan and containing histidine (SD/-Leu/-Trp/+His) plates (low-stringency plate). The transformants were picked up and spotted onto selective medium lacking histidine (SD/-Leu/-Trp/-His) plates with 0.2, 0.5, 1.0, 2.0, or 5.0 mmol/L 3-amino-1,2,4-triazole (3-AT), a competitive inhibitor of the HIS3 reporter gene (high-stringency plate) and plates without 3-AT (medium-stringency plate). The plates were then incubated at 30°C for 4 days, and the growth of the transformants was analyzed.

Immunoprecipitation and Immunoblot Analysis

For expression in mammalian cells, wtMYOT or mMYOT inserted in pGADT7 were digested by *Eco*RI and *Bam*HI, and ligated into FLAG-tag-inserted pcDNA3.1/V5-HisA (kindly gifted by Dr Ishiura, University of Tokyo). The cDNAs inserted in pGADT7 were also digested by *Sfi*I and *Xho*I and ligated into pCMV-Myc vector (Takara Bio).

COS-7 cells were cultured in Dulbecco modified Eagle medium (Sigma, St Louis, MO) supplemented with 10% fetal bovine serum (Invitrogen, Carlsbad, CA) at 37°C in a humidified atmosphere of 5% carbon dioxide. The cells were transiently transfected using FuGENE HD transfection reagent (Roche Diagnostics, Indianapolis, IN) according to the manufacturer's instructions. Mouse horseradish peroxidase–conjugated anti-Myc antibody (9E10) was purchased from Santa Cruz Biotechnology (Santa Cruz, CA). Rabbit anti-FLAG polyclonal antibody was purchased from Sigma.

COS-7 cells were cotransfected with 5 μg of each plasmid. Forty-eight hours after transfection, the cells were then lysed in 1.0 mL of lysis buffer containing 20 mmol/L Tris-HCl (pH 7.5), 150 mmol/L NaCl, 10 mmol/L EDTA (pH 8.0), 10% glycerol, 1% Nonidet P-40, and Complete Protease Inhibitor Cocktail (Roche Diagnostics). The lysates were incubated at 4°C for 30 minutes with gentle rotation and then centrifuged at 15,000 × *g* at 4°C for 30 minutes. The supernatants were collected, and their protein concentrations were determined using the protein assay kit (Bio-Rad, Hercules, CA).

For immunoprecipitation, the protein concentration of the cleared lysates was adjusted to 1.5 μg/μL, and anti-FLAG M2 affinity gel (Sigma) was added. The mixtures were incubated at 4°C overnight. The resulting immune complexes were washed once with lysis buffer and 3 times with Tris buffered saline. The proteins were eluted by boiling at 95°C for 5 minutes in the sample buffer without reducing agent (50 mmol/L Tris-HCl [pH 6.8], 2% sodium dodecyl sulfate, 1% glycerol [vol/vol], 0.1% bromophenol blue), and resolved by sodium dodecyl sulfate–polyacrylamide gel electrophoresis. The polyacrylamide gel electrophoresis–separated proteins were transferred to Immobilon-P membranes (Millipore, Bedford, MA), and the membranes were blocked with blocking buffer (5% nonfat dry milk in PBS containing 0.05% Tween-20) at room temperature for 1 hour. The blocked membranes were incubated with a primary antibody at room temperature for 1 hour. Anti-Myc-horseradish peroxidase antibody was diluted in Can Get Signal solution 2 (Toyobo, Osaka, Japan) at 1:1000. Anti-FLAG polyclonal antibody was diluted in blocking buffer at 1:4000) Anti-FLAG was followed with horseradish peroxidase–conjugated anti-rabbit immunoglobulin G antibody at 1:4000 at room temperature for 30 minutes. Immunoreactive complexes on the membranes were visualized using enhanced chemiluminescence or enhanced chemiluminescence–plus detection reagent (GE Healthcare UK Ltd, Buckinghamshire, UK).

RESULTS

Genetic Analysis

We identified a novel heterozygous missense mutation c.1214G>A (p.R405K) in Exon 9 of *MYOT* in 1 LGMD patient (Fig. 1B). This mutation was not identified in a panel of 100 healthy Japanese controls.

Clinical Data

The 57-year-old female patient presented with gait disturbance. She started experiencing difficulty in standing up and climbing the stairs by age 41 years. Her condition gradually progressed, and by age 50 years, she could not walk long distances and could not stand up or climb stairs without support. Her deceased father and elder sister had a similar condition. Her sister was previously diagnosed as having sporadic inclusion body myositis, but further information could not be obtained. On examination, the patient had proximal dominant muscle weakness, especially in neck flexors, iliopsoas, hamstring, and quadriceps muscles (3/5 by

manual muscle test), but no facial muscle weakness. She also showed a waddling gait and decreased deep tendon reflexes. Serum creatine kinase was mildly elevated (385 IU/L; normal, <200 IU/L).

Histochemical and Immunohistochemical Analyses

Muscle tissue from the patient's vastus lateralis muscle showed marked variation in fiber size, scattered fibers with internally placed nuclei, and small angular fibers. There were scattered fibers with rimmed vacuoles (Fig. 2A). No obvious protein aggregates were seen. The intermyofibrillar networks were disorganized (Fig. 2B). Myosin ATPase staining showed an increase in the percentage of type 2C fibers (7%).

By immunohistochemistry, strongly immunoreactive aggregates of myotilin, αB-crystallin, ZASP, desmin (Figs. 2C–F), and actin (data not shown) were observed in a few fibers. Immunohistochemical and immunoblotting studies excluded other diagnosable causes of LGMD.

Immunoblotting Analysis of Myotilin

The patient's muscle specimen showed an increased intensity of the 57-kd band corresponding to the amount of myotilin monomers compared with the band intensity in a control sample. On the other hand, the 110-kd band corresponding to myotilin dimer was fainter in the patient's sample than in the control muscle (Fig. 2G).

Y2H Analysis for the MYOT Mutation

To determine the effect of the p.R405K mutation on protein-protein interactions, we used a Y2H system. We first tested the homodimerization capacity of wild and mutant myotilin. We generated *GAL4* DNA-binding domain or activation domain constructs containing wtMYOT or mMYOT and cotransformed them to yeast. All MYOT double transformants grew on low-stringency plates, indicating that no MYOT constructs were intrinsically lethal to the yeast cells. Only wtMYOT double transformant grew on medium- and high-stringency plates; the wtMYOT and mMYOT transformant and the mMYOT double transformant did not grow. These results indicate defective dimerization of mutant myotilin with both wild-type and mutant myotilin.

We next tested the interaction between myotilin and its known binding protein partners ACTA1, ACTN2, and FLNC. We cotransformed yeast with wtMYOT or mMYOT with each of ACTA1, ACTN2, and FLNC. The wtMYOT and ACTA1, mMYOT and ACTA1, wtMYOT and ACTN2, and wtMYOT

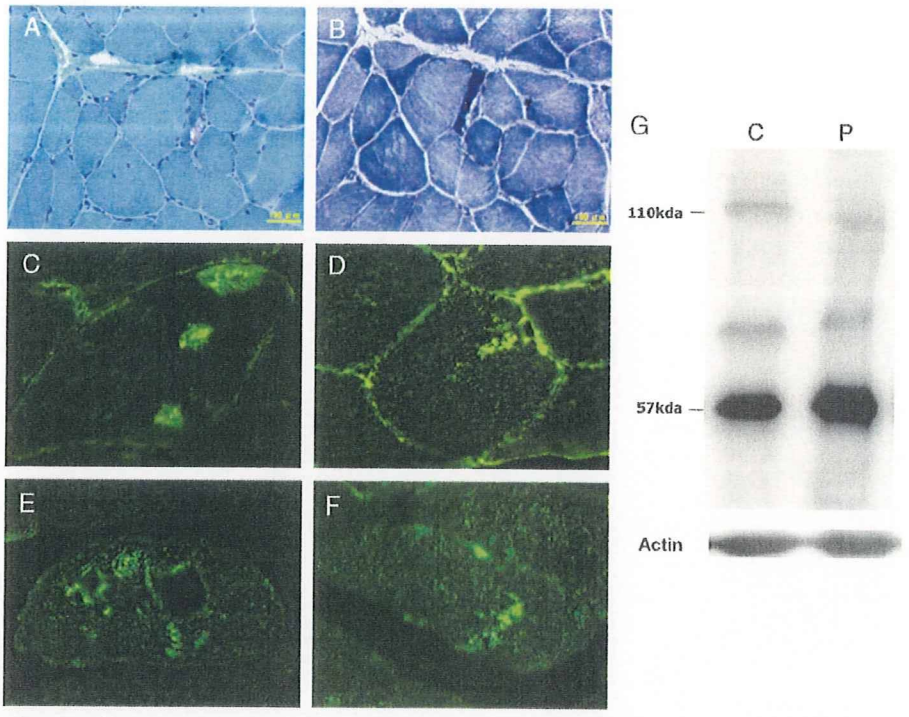

FIGURE 2. Histopathology and immunoblot of muscle from patient with p.R405K mutation. **(A)** Modified Gomori trichrome stain shows scattered fibers with rimmed vacuoles. **(B)** Nicotinamide adenine dinucleotide dehydrogenase–tetrazolium reductase stain shows myofibrillar disorganization. **(C–F)** Immunostaining reveals abnormal accumulation of myotilin **(C)**, desmin **(D)**, Z band alternatively spliced PDZ motif protein **(E)**, and αB-crystallin **(F)**. **(G)** Immunoblot analysis of myotilin in muscle from the patient shows an increased intensity of the 57-kd band that corresponds to monomeric myotilin and a decrease in intensity of the 110-kd band that corresponds to myotilin dimer compared with the control muscle sample. Scale bars = **(A, B)** 100 μm; **(C–F)** 20 μm. C, control; P, patient.

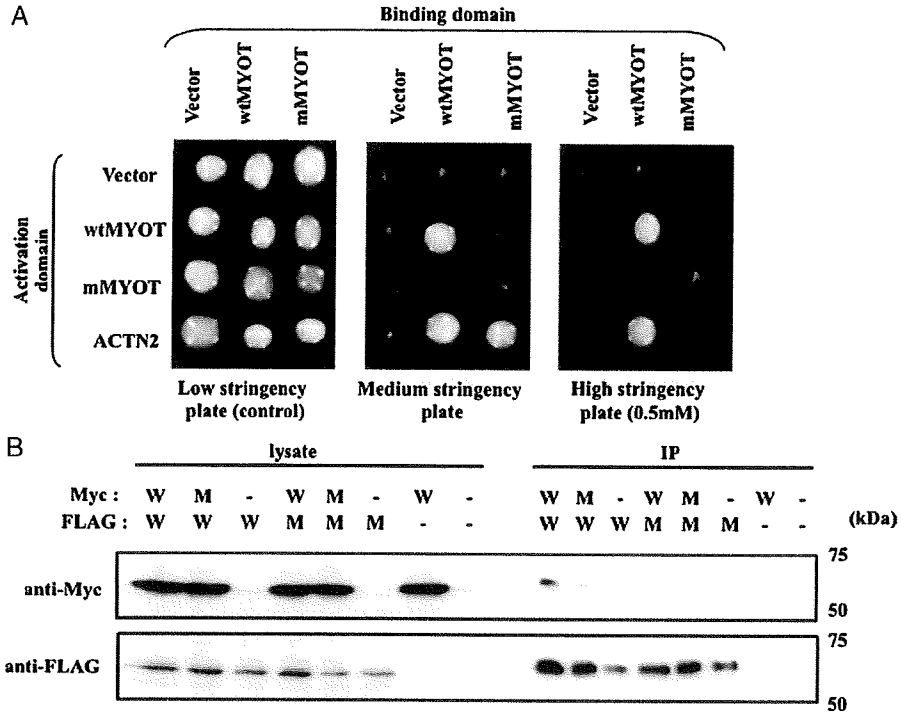

FIGURE 3. Defective homodimerization of mutant myotilin. **(A)** Yeast cells were cotransformed with expression plasmids containing Gal4 DNA-binding or activation domains alone (vector) or fused in frame to full-length human wild-type myotilin (wtMYOT), mutant myotilin (mMYOT), or α-actinin (ACTN2). Double transformants were first selected on low-stringency plates (used as control) and then spotted onto medium- and high-stringency plates. There is a lack of growth of cells coexpressing mMYOT and the corresponding constructs containing mMYOT and wtMYOT on medium- and high-stringency plates (0.5 mmol/L 3-amino-1,2,4-triazole [3-AT]). Cells cotransformed with mMYOT and ACTN2 did not grow on high-stringency plates (0.5 mmol/L 3-AT). **(B)** Myc-tagged myotilin and FLAG-tagged myotilin were coexpressed in COS-7 cells. The cell lysates were subjected to immunoprecipitation with an anti-FLAG M2 affinity gel. The immunoprecipitates (IP) were detected with anti-Myc (upper) or anti-FLAG (lower) antibodies. The mMYOT shows reduced interaction with both wild-type (W) and mutant (M) myotilin. −, empty vector transfected as a control.

and FLNC transformants grew on medium- and high-stringency plates (0.2–2 mmol/L 3-AT). By contrast, mMYOT and ACTN2 transformants grew on medium-stringency and high-stringency plates with 0.2 mmol/L 3-AT but did not grow on high-stringency plates with 0.5, 1, or 2 mmol/L 3-AT (Fig. 3A). This result indicates a decreased binding ability of mutant myotilin to α-actinin. In addition, mMYOT and FLNC transformants did not grow on medium- or high-stringency medium, but FLNC and mMYOT transformants grew on high-stringency medium when Gal4 DNA-binding domain construct containing FLNC was used as the bait (data not shown).

Immunoprecipitation Analysis of Homodimerization

We next used coimmunoprecipitation analysis to confirm the homodimerization defect of mutant myotilin. Myc-tagged wild-type myotilin (Myc-wtMYOT) coimmunoprecipitated with FLAG-tagged wild-type myotilin (FLAG-wtMYOT); this indicates that wild-type myotilin forms a homodimer. On the other hand, other combinations of FLAG-wtMYOT and Myc-tagged mutant myotilin (Myc-mMYOT), FLAG- mMYOT and Myc-wtMYOT, and FLAG-mMYOT and Myc-mMYOT showed decreased interaction (Fig. 3B). These results suggest that the p.R405K mutation in the second immunoglobulin-like domain of myotilin can affect the homodimerization ability of myotilin protein.

DISCUSSION

Limb girdle muscular dystrophy type 1A is an autosomal-dominant muscular dystrophy characterized by progressive proximal muscle weakness and wasting. Distal muscle weakness may occur later (12, 13). The *MYOT* mutations are known to cause LGMD1A, but only a few genetically confirmed LGMD1A patients have been reported to date. Here, we report the first *MYOT* mutation in the Japanese population. The patient had a clinical severity similar to that in other reported LGMD1A patients, and there was also disorganization of myofibrils and rimmed vacuoles in the muscle biopsy tissue. Immunohistochemical analysis revealed accumulation of Z disk proteins (i.e. myotilin, αB-crystallin, ZASP, desmin, and actin) as seen in MFM, thus highlighting the similarities in the pathology of LGMD1A and MFM (21).

Myotilin has 2 immunoglobulin domains in the C terminus of the molecule. Several cytoskeletal proteins have been shown to contain immunoglobulin domains, and most of these proteins are specifically expressed in striated muscle, suggesting a special function for the immunoglobulin domains in this tissue (13, 22). Immunoglobulin domains are known to mediate protein-protein interactions and to serve as dimerization sites and regulators for molecular elasticity and act as modular "spacers" that place an interacting module in the correct position for performing its function (1, 7, 22, 23). The functional importance of the immunoglobulin domains in myotilin was demonstrated by introducing myotilin with mutant immunoglobulin domains in yeast cells that do not express endogenous myotilin (5); these immunoglobulin domains are the site for homodimerization necessary for the actin bundling (8). Our data indicate that the immunoglobulin domains in the C terminus are responsible for the actin binding and bundling ability of myotilin (Fig. 3B).

All previously reported disease-related mutations in *MYOT* are located in the serine-rich amino-terminus of myotilin. The novel p.R405K mutation we identified is located in the second immunoglobulin domain of myotilin, which is important for homodimeric formation and interaction with other proteins (Fig. 1A) (1, 5, 6); this region is highly conserved in vertebrate species, including the mutated residue (Fig. 1B). We found that the 110-kd myotilin dimer band was faint in the patient's muscle sample by immunoblotting, although, as in a previous report (24), the amount of myotilin in the patient's muscle sample was increased. Furthermore, the decreased homodimerization ability of mutant (p.R405K) myotilin was confirmed by the Y2H and immunoprecipitation studies in which interactions of mutant myotilin with both wild-type and mutant myotilin were greatly reduced (Figs. 3A, B). These results suggest that the disturbance of homodimerization caused by the mutated allele may affect the actin-bundling ability of myotilin at the Z disks, resulting in decreased filament stability and gradual disruption in the Z disk in vivo.

Myotilin interacts with 2 important actin-bundling (cross-linker) proteins (i.e. α-actinin and FLNC), forming a complex of 3 actin bundlers at the Z disk. Previous experiments have shown that myotilin enhances the binding of α-actinin to actin (8). The decreased binding ability of mutated myotilin to α-actinin we observed suggests that this altered interaction may loosen the complex formed by these actin bundler proteins leading to a decrease in strength and ability of the Z disk to resist mechanical stress during muscle contraction. On the other hand, mutant myotilin showed no apparent defect in interaction with actin but questionable defective interaction with FLNC by Y2H assay; this issue requires further analysis.

Several hypotheses have been proposed regarding the pathogenesis of the previously reported *MYOT* mutations in Exon 2, including the fact that the serine-rich domain contains a hydrophobic stretch that mediates the localization of small amounts of myotilin to the sarcolemmal membrane. *MYOT* mutations may elongate this hydrophobic stretch, possibly disturbing its interactions with the sarcolemmal membrane (12). It has also been suggested that these mutations may disrupt the binding of myotilin with α-actinin, FLNC, or a novel protein-binding partner (12). None of these hypotheses have been proven. Disease-associated substitutions in myotilin did not affect the localization or actin-bundling ability of myotilin, suggesting that the pathogenic mechanism of the myotilin mutations examined may be independent of its actin-modulating effects (5). In contrast to the previously reported mutations (5, 13), ours is the first report to demonstrate a functional abnormality caused by mutated myotilin. Our data suggest that the p.R405K missense mutation disrupts myotilin homodimerization and decreases the interaction between myotilin and α-actinin, which subsequently may affect its actin-bundling ability.

ACKNOWLEDGMENTS

The authors thank Dr O. Carpén (University of Helsinki) for the kind gift of anti-myotilin antibody and Dr S. Ishiura (University of Tokyo) for providing the FLAG-inserted pcDNA3.1 V5/HisA vector. The authors also thank Dr R. Gabor (National Center of Neurology and Psychiatry) for his help in the Y2H assay.

REFERENCES

1. Salmikangas P, Mykkanen OM, Gronholm M, et al. Myotilin, a novel sarcomeric protein with two Ig-like domains, is encoded by a candidate gene for limb-girdle muscular dystrophy. Hum Mol Genet 1999;8:1329–36
2. Parast MM, Otey CA. Characterization of palladin, a novel protein localized to stress fibers and cell adhesions. J Cell Biol 2000;150:643–56
3. Mykkanen OM, Gronholm M, Ronty M, et al. Characterization of human palladin, a microfilament-associated protein. Mol Biol Cell 2001;12:3060–73
4. Bang ML, Mudry RE, McElhinny AS, et al. Myopalladin, a novel 145-kilodalton sarcomeric protein with multiple roles in Z-disc and I-band protein assemblies. J Cell Biol 2001;153:413–27
5. von Nandelstadh P, Gronholm M, Moza M, et al. Actin-organising properties of the muscular dystrophy protein myotilin. Exp Cell Res 2005;310:131–39
6. van der Ven PF, Wiesner S, Salmikangas P, et al. Indications for a novel muscular dystrophy pathway. Gamma-filamin, the muscle-specific filamin isoform, interacts with myotilin. J Cell Biol 2000;151:235–48
7. Gontier Y, Taivainen A, Fontao L, et al. The Z-disc proteins myotilin and FATZ-1 interact with each other and are connected to the sarcolemma via muscle-specific filamins. J Cell Sci 2005;118:3739–49
8. Salmikangas P, van der Ven PF, Lalowski M, et al. Myotilin, the limb-girdle muscular dystrophy 1A (LGMD1A) protein, cross-links actin filaments and controls sarcomere assembly. Hum Mol Genet 2003;12:189–203
9. Selcen D, Engel AG. Mutations in myotilin cause myofibrillar myopathy. Neurology 2004;62:1363–71
10. Foroud T, Pankratz N, Batchman AP, et al. A mutation in myotilin causes spheroid body myopathy. Neurology 2005;65:1936–40
11. Olivé M, Goldfarb LG, Shatunov A, et al. Myotilinopathy: Refining the clinical and myopathological phenotype. Brain 2005;128:2315–26
12. Hauser MA, Conde CB, Kowaljow V, et al. Myotilin mutation found in second pedigree with LGMD1A. Am J Hum Genet 2002;71:1428–32
13. Hauser MA, Horrigan SK, Salmikangas P, et al. Myotilin is mutated in limb girdle muscular dystrophy 1A. Hum Mol Genet 2000;9:2141–47
14. Penisson-Besnier I, Talvinen K, Dumez C, et al. Myotilinopathy in a family with late onset myopathy. Neuromuscul Disord 2006;16:427–31
15. Berciano J, Gallardo E, Dominguez-Perles R, et al. Autosomal dominant distal myopathy with a myotilin S55F mutation: Sorting out the phenotype. J Neurol Neurosurg Psychiatry 2008;79:205–8

16. Schröder R, Reimann J, Salmikangas P, et al. Beyond LGMD1A: Myotilin is a component of central core lesions and nemaline rods. Neuromuscul Disord 2003;13:451–55
17. Matsumoto H, Hayashi YK, Kim DS, et al. Congenital muscular dystrophy with glycosylation defects of alpha-dystroglycan in Japan. Neuromuscul Disord 2005;15:342–48
18. Starcevic M, Dell'Angelica EC. Identification of snapin and three novel proteins (BLOS1, BLOS2, and BLOS3/reduced pigmentation) as subunits of biogenesis of lysosome-related organelles complex-1 (BLOC-1). J Biol Chem 2004;279:28393–401
19. Falcon-Perez JM, Starcevic M, Gautam R, Dell'Angelica EC. BLOC-1, a novel complex containing the pallidin and muted proteins involved in the biogenesis of melanosomes and platelet-dense granules. J Biol Chem 2002;277:28191–99
20. Mitsuhashi H, Futa E, Sasagawa N, et al. Csk-homologous kinase interacts with SHPS-1 and enhances neurite outgrowth of PC12 cells. J Neurochem 2008;105:101–12
21. Selcen D. Myofibrillar myopathies. Curr Opin Neurol 2008;21:585–99
22. Vaughan KT, Weber FE, Einheber S, et al. Molecular cloning of chicken myosin-binding protein (MyBP) H (86-kDa protein) reveals extensive homology with MyBP-C (C-protein) with conserved immunoglobulin C2 and fibronectin type III motifs. J Biol Chem 1993;268:3670–76
23. Fucini P, Renner C, Herberhold C, et al. The repeating segments of the F-actin cross-linking gelation factor (ABP-120) have an immunoglobulin-like fold. Nat Struct Biol 1997;4:223–30
24. Barrachina M, Moreno J, Juves S, et al. Target genes of neuron restrictive silencer factor are abnormally up-regulated in human myotilinopathy. Am J Pathol 2007;171:1312–23

[Autophagy 5:6, 795-804; 16 August 2009]; ©2009 Landes Bioscience

Research Paper

Autophagic degradation of nuclear components in mammalian cells

Young-Eun Park,[1,2] Yukiko K. Hayashi,[1,*] Gisèle Bonne,[3,4] Takuro Arimura,[5] Satoru Noguchi,[1] Ikuya Nonaka[1] and Ichizo Nishino[1]

[1]Department of Neuromuscular Research; National Institute of Neuroscience; National Center of Neurology and Psychiatry (NCNP); Kodaira, Tokyo Japan; [2]Department of Neurology and Medical Research Institute; Pusan National University Hospital; Seo-gu, Busan Korea; [3]Inserm-UPMC-CNRS UMRS_974; Institut de Myologie Paris; France; [4]AP-HP; Groupe Hospitalier Pitié-Salpêtrière; U.F. Cardiogénétique et Myogénétique; Service de Biochimie Métabolique; Paris, France; [5]Department of Molecular Pathogenesis; Medical Research Institute; Tokyo Medical and Dental University; Tokyo, Japan

Abbreviations: DAPI, 4',6-diamidino-2-phenylindole; GFP, green fluorescent protein; LC3, microtubule-associated protein 1 light chain 3; LC3-I, unlipidated form of LC3; LC3-II, lipidated form of LC3 (LC3-phopholipid conjugate); PI3K, phosphatidylinositol-3 kinase

Key words: autophagy, nuclear envelopathies, A-type lamins, emerin, nucleus

Autophagy is an evolutionarily conserved intracellular mechanism for the degradation of organelles and proteins. Here we demonstrate the presence of perinuclear autophagosomes/autolysosomes containing nuclear components in nuclear envelopathies caused by mutations in the genes encoding A-type lamins (*LMNA*) and emerin (*EMD*). These autophagosomes/autolysosomes were sometimes bigger than a nucleus. The autophagic nature is further supported by upregulation of LC3-II in $Lmna^{H222P/H222P}$ fibroblasts. In addition, inhibition of autophagy led to the accumulation of nuclear abnormalities and reduced cell viability, strongly suggesting a beneficial role of autophagy, at least in these cells. Similar giant autophagosomes/autolysosomes were seen even in wild-type cells, albeit rarely, implying that this "nucleophagy" is not confined to the diseased condition, but may be seen even in physiologic conditions to clean up nuclear wastes produced by nuclear damage.

Introduction

Nuclear envelopathies refer to disorders caused by mutations in the genes encoding nuclear envelope proteins, such as A-type lamins (*LMNA*) and emerin (*EMD*). *LMNA* mutations are known to cause a heterogeneous group of disorders collectively called as laminopathies, which encompass autosomal dominant and recessive forms of Emery-Dreifuss muscular dystrophy (AD and AR-EDMD), limb girdle muscular dystrophy type 1B (LGMD1B), cardiomyopathy with conduction defects, partial lipodystrophy, Charcot-Marie-Tooth disease type 2, and premature aging syndrome.[1-9] *EMD* mutations are causative for emerinopathies, a group of disorders that include X-linked EDMD, LGMD, cardiomyopathy with conduction defects, and familial atrial fibrillation.[10-13]

Because lamins form a protein meshwork of nuclear lamina at the nucleoplasmic side of inner nuclear membrane and have an important role in the maintenance of nuclear architecture, mutations in *LMNA* are thought to cause nuclear membrane fragility. This phenomenon is expected especially in skeletal and cardiac muscle cells which are constantly subjected to repeated mechanical stress. Loss of A-type lamins has been implicated to impair nuclear mechanics and increase nuclear fragility.[14,15] Loss of emerin, an inner nuclear membrane protein, could also lead to structural instability of nuclear membrane; emerin binds to several structural proteins in nucleus such as lamins, nesprins and nuclear actin, and can promote actin polymerization in vitro.[16-19]

In skeletal and cardiac muscles from patients with laminopathy and emerinopathy, various nuclear abnormalities have been observed, which are mainly composed of alteration in nuclear shape and emphasizing the role of lamins in the maintenance of nuclear integrity.[20-24] We recently demonstrated the presence of unique perinuclear vacuolar structures in the skeletal and/or cardiac muscles from laminopathy patients and emerin-null mice under electron microscopy,[21,25] but neither the nature of these structures nor their role in disease pathomechanism have ever been clarified. As most of these vacuolar structures contained amorphous and electron-dense materials resembling myelinated materials, we suspected that these are actually autophagic in nature.

Macroautophagy is a well-conserved molecular mechanism for the bulk degradation of organelles and proteins.[26-28] During autophagic process a double-membraned structure, the so-called phagophore or preautophagosome, randomly engulfs cytosolic components and cellular organelles. It is enclosed to form the so-called autophagosome, which is then fused with lysosome enabling intra-autophagosomal components to be degraded by lysosomal hydrolases.[28]

Recently it has been alluded to that the autophagic process is also responsible for selective degradation of specific cellular

*Correspondence to: Yukiko K. Hayashi; National Institute of Neuroscience, NCNP; 4-1-1 Ogawa-Higashi; Kodaira, Tokyo 187-8502 Japan; Tel.: 81.42.341.2711 Ex. 5113; Fax: 81.42.346.1742; Email: hayasi_y@ncnp.go.jp

Submitted: 11/17/08; Revised: 04/20/09; Accepted: 04/30/09

Previously published online as an *Autophagy* E-publication:
http://www.landesbioscience.com/journals/autophagy/article/8901

components; for instance, pexophagy works to decrease the number of peroxisome adapting to environmental changes in yeast, while mitophagy and ER-phagy have been suggested to degrade damaged mitochondria and overstressed endoplasmic reticulum, respectively.[29-31]

In this study, we show that the perinuclear vacuolar structures are actually giant autophagosomes/autolysosomes involved in the degradation of damaged nuclear components, extending the concept of macroautophagy in various cellular organelles to include the nucleus.

Results

Perinuclear vacuolar structures observed in skeletal and cardiac muscles of human and mouse nuclear envelopathy. Electron microscopic observation of skeletal muscles from patients with laminopathy revealed perinuclear vacuolar structures in ~10% of myonuclei.[21] Most of these structures were consistently found in close proximity to the irregularly-shaped nuclei which also contained disorganized chromatin structures. These vacuolar structures varied in size from 1.5 to 5 μm in diameter, and were observed to contain either diffuse granular, honeycomb-like or dense amorphous materials within multiple layered and folded membranes (Fig. 1A and B). Similar structures were also observed near the nuclei of nonmuscle cells from muscle specimens (Fig. 1C).

Perinuclear vacuolar structures were also detected in skeletal and cardiac muscles from different mouse models of nuclear envelopathies including emerin lacking *Emd*$^{-/-}$ (89 weeks of age),[25] A-type lamin-deficient *Lmna*$^{-/-}$ (10 weeks), and homozygous knock-in *Lmna*$^{H222P/H222P}$ (24 weeks) mouse models (Fig. S1), and also in skin fibroblasts from 10-week-old *Lmna*$^{H222P/H222P}$ mouse (Fig. 1D).

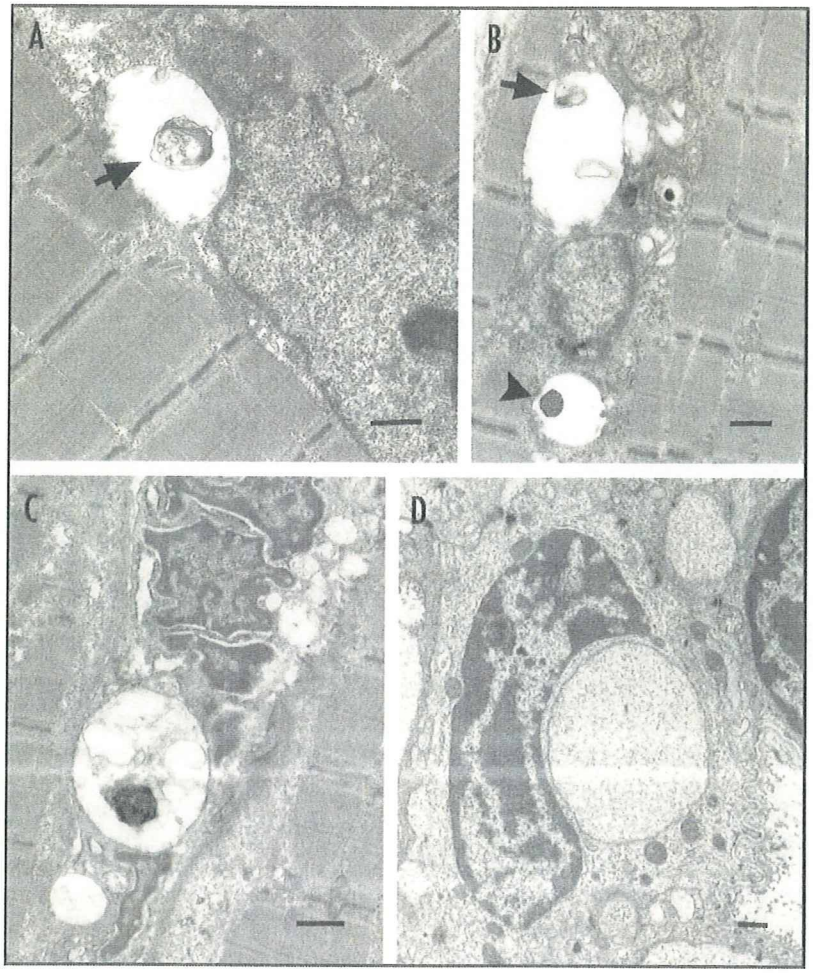

Figure 1. Electron microscopic observation of perinuclear vacuolar structures in skeletal muscles from patients (A–C) and skin from *Lmna*$^{H222P/H222P}$ mouse (D). (A–C) Perinuclear vacuolar structures of variable diameter usually contain myelinated (arrows) and dense amorphous materials (arrowhead) in muscle (A and B) and nonmuscle cells in skeletal muscle specimens (C) of patients with AD-EDMD/LGMD1B. (D) In the skin obtained from 10-week-old *Lmna*$^{H222P/H222P}$ mouse, similar perinuclear vacuolar structures are observed. Bars, 0.5 μm.

Electron microscopic observation of *Lmna*$^{H222P/H222P}$ MEF. For further characterization of nuclear changes, we used mouse embryonic fibroblasts (MEF) obtained from *Lmna*$^{H222P/H222P}$ mice. In these cells, nuclei had markedly irregular shape, and in addition small particles with similar electron density to nucleus were seen (Fig. 2A, arrow). In some areas, there was blurring of the nuclear membrane, probably suggesting the disruption of nuclear membrane, where small circular structures were accumulated (Fig. 2A, arrowheads). Vacuolar structures from 3 to 7 μm in diameter were frequently found in the cytoplasm, especially near the blurred nuclear membrane, and appeared to fuse with one another (Fig. 2B). These vacuolar structures were mostly single- or double-membraned although in some cases it was difficult to recognize clear membranous structures (Fig. 2B and C). Smaller electron-dense vesicles were also much increased over the cytoplasm but more highlighted around large vacuolar structures (Fig. 2C and D). The contents of vacuolar structures were variable from granular substances to pieces of amorphous materials, but a few were empty (Fig. 2E–H).

Nuclear shape of cultured *Lmna*$^{H222P/H222P}$ MEF. To characterize perinuclear vacuolar structures by in vitro analysis, we performed immunocytochemistry on *Lmna*$^{H222P/H222P}$ MEF using antibodies against nuclear envelope proteins (e.g., lamins A, C and B, emerin and LAP2). The nuclei had markedly irregular shape and, in addition, single or multiple blebs and nuclear herniation were seen in 21 ± 1.8% of *Lmna*$^{H222P/H222P}$ cells (Fig. S2), similar to previous reports on fibroblasts from patients with *LMNA* mutations.[32,33] Nuclear envelope proteins were intensely stained at bleb sites (Fig. S2, arrowheads). Moreover, various-sized DAPI positive particles were often identified in the cytoplasm around nuclei

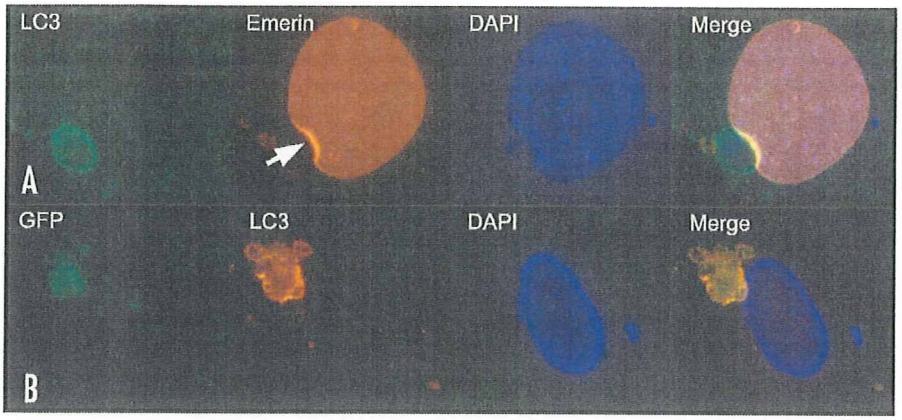

Figure 2. Electron microscopic findings of perinuclear vacuolar structures in *Lmna*$^{H222P/H222P}$ MEF. (A) A particle with similar electron density to the nucleus is detected near the nucleus (arrow). A part of nuclear membrane is blurred suggesting the disruption of nuclear membrane, where small circular structures are present (arrowheads). Vacuolar structures are identified near the nucleus, especially around the ruptured nuclear membrane. (B–D) Some cells contained multiple double- or single-membraned vacuolar structures together with electron dense smaller vesicles. (E–H) The contents of vacuolar structures are variable showing granular substances that fills the whole vacuole, or pieces of amorphous particles. A few are empty. Bars, 0.5 μm.

(Fig. S2, arrows). On the other hand, most of the wild-type cells displayed clearly round shape of nuclei; small blebs were identified only in less than 1% of the cells, and DAPI-positive particles were rarely seen outside nuclei.

Round-shaped LC3-positive signals close to the nuclei in *Lmna*$^{H222P/H222P}$ MEF. As we have insinuated that the vacuolar structures near the nuclei observed under electron microscope could be autophagic in nature, we performed immunocytochemical analysis of microtubule-associated protein 1/light chain 3 (LC3) in *Lmna*$^{H222P/H222P}$ fibroblasts. LC3 is a homologue of yeast Atg8 and is commonly used as a marker of autophagy because it decorates inner and outer membranes of autophagosome.[34] In about 10% of *Lmna*$^{H222P/H222P}$ cells, characteristically round LC3-positive signals were detected near or attached to the nucleus. The part of nuclear membrane interfacing with LC3-staining was sometimes strongly stained with lamins and emerin (Fig. 3A, arrow). Similar findings were also observed in *Lmna*$^{-/-}$ fibroblasts.

Large-sized, round-shaped GFP staining close to nuclei in *Lmna*$^{H222P/H222P}$*/GFP-LC3* MEF. To further characterize the autophagic nature of these perinuclear structures, we produced *Lmna*$^{H222P/H222P}$*/GFP-LC3* transgenic mice. Green fluorescent protein-tagged-LC3 (GFP-LC3) transgenic mouse model has been developed for in vivo analysis of autophagy.[35] On immunocytochemistry, MEF from *Lmna*$^{H222P/H222P}$*/GFP-LC3* mice showed similar frequency of abnormally-shaped nuclei to *Lmna*$^{H222P/H222P}$ cells. In addition, perinuclear round GFP-positive staining, sometimes bigger than the nuclei, were detected in about 10% of observed cells whereas it was rarely seen in wild-type/*GFP-LC3* cells under similar standard culture condition. In addition, these GFP-positive perinuclear signals were almost completely colocalized with LC3 in *Lmna*$^{H222P/H222P}$*/GFP-LC3* cells (Fig. 3B), being diffusely distributed over or outlining GFP signal.

As the activation of autophagy is induced by the upregulation of certain molecules, we examined the expression of other known autophagy-related proteins in *Lmna*$^{H222P/H222P}$*/GFP-LC3* fibroblasts to know whether similar machinery to macroautophagy is working in these cells. In a considerable number of cells, the perinuclear GFP-positive signals colocalized with Atg5 and Atg16L (Fig. 4A), which are known to participate in the initiation of phagophore (or preautophagosome) formation in mammalian cells.[36] Along the border of the perinuclear GFP-positive signals, we observed positive immunoreaction to Atg9 (Fig. 4B), which is associated with phagophore expansion.[37] The GFP signals also colocalized with Rab7 (Fig. 4C), which is known as a small GTPase protein associated with autophagosome maturation.[38] We also checked the involvement of lysosomes, and found that LAMP2, a lysosomal membrane protein, was identified around and inside GFP-positive staining (Fig. 4D); this finding was confirmed by the colocalization of GFP signals with Lyso-Tracker® which marks lysosmes (Fig. 4E). With these findings, we can consider that the large perinuclear GFP signals are giant autophagosomes/autolysosomes.

Intriguingly, GFP-positive autophagosomes/autolysosomes contained extranuclear DAPI with variable staining intensity from intense to blurred or faint (Figs. 3–5). These DAPI signals were colocalized with histone H1 (Fig. 5A), but were rarely co-stained with nuclear envelope proteins such as lamin A and B (Fig. 5B and C), indicating that these are actually extranuclear and may indicate damaged DNA. We therefore immunostained with anti-γH2AX, a marker of DNA double-strand breaks caused by various insults which is known to have certain roles in the recognition and repair of damaged DNA.[39] Some of the extranuclear DAPI signal was colocalized with γH2AX and contained in GFP-positive autophagosomes/autolysosomes (Fig. 5D, arrowhead). γH2AX was detected also in intranuclear portions, mainly in bleb sites (data not shown). These results suggest that extranuclear damaged DNA is destined for autophagic degradation. On the other hand, we could not find any overlap staining of LC3 and DAPI in rarely observed markedly fragmented nuclei with γH2AX staining, although LC3 positive signals can be seen in the cytoplasm (Fig. 5E).

Notably, in wild-type/*GFP-LC3* cells, similar autophagosomes/autolysosomes containing extranuclear DAPI signals were likewise observed, but with rare frequency of less than 0.1%.

Both LC3-II protein amount and transcriptional level of Maplc3b were increased in *Lmna*$^{H222P/H222P}$ MEF. On immunoblotting analysis, the protein amount of LC3-II, which is a lipidated form of LC3 and a marker of autophagosome formation, was significantly increased in *Lmna*$^{H222P/H222P}$ compared

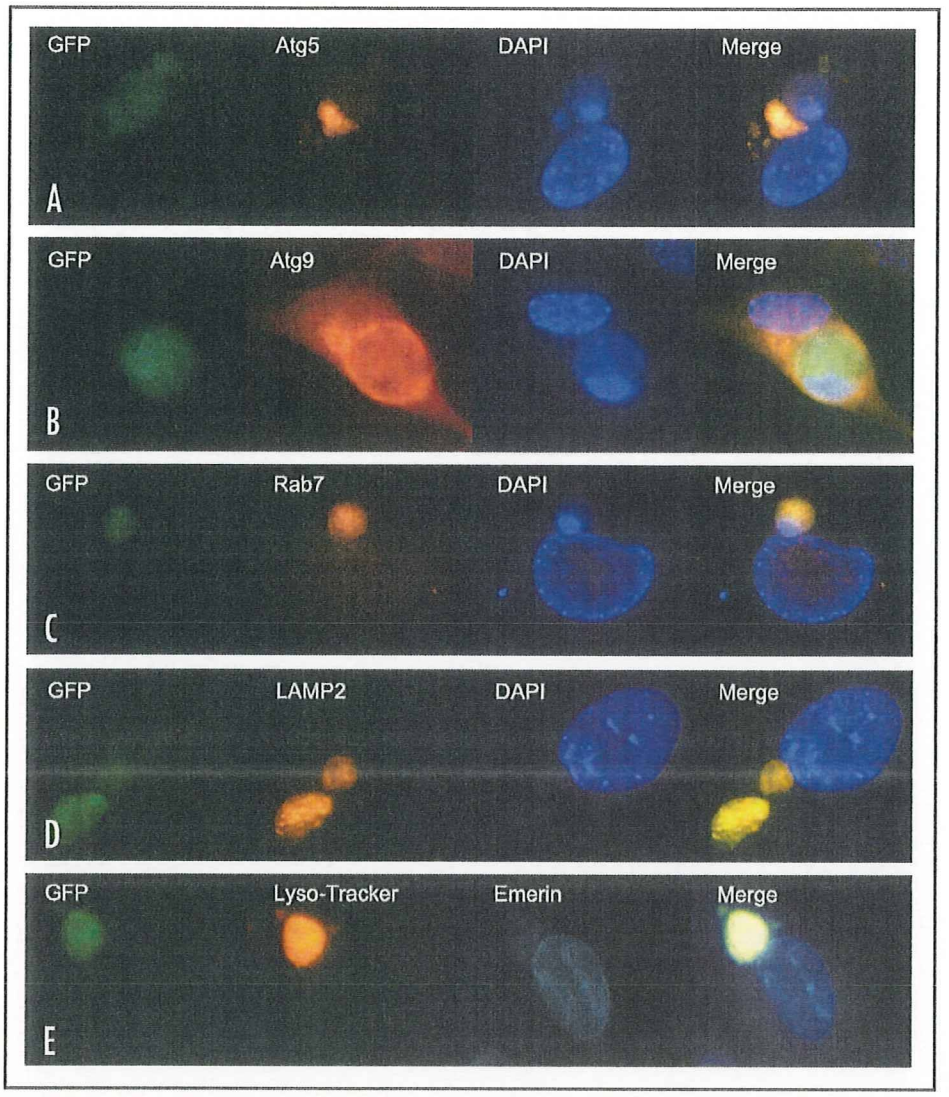

Figure 3. Perinuclear LC3 staining in *Lmna*$^{H222P/H222P}$ and *Lmna*$^{H222P/H222P}$/*GFP-LC3* MEFs. (A) In *Lmna*$^{H222P/H222P}$ MEF, a large-sized and round-shaped LC3-positive vacuolar structure is seen with stronger marginal dot-like staining. DAPI-positive materials are included within. Emerin is more strongly stained in the part of nuclear membrane interfacing with the LC3-positive structures (arrow). (B) In *Lmna*$^{H222P/H222P}$/*GFP-LC3* MEF, LC3 signal is detected with the GFP.

with wild-type cells (Fig. 6A). Because an increased amount of LC3-II could be interpreted either as increased autophagy influx or blocked autophagosome maturation,[40] we quantified the amount of LC3-II with or without lysosomal protease inhibitors (pepstatin A and E64d). LC3-II in *Lmna*$^{H222P/H222P}$ cells was much increased with lysosomal inhibitors (Fig. 6A), implying that the increased LC3-II amount is due to enhanced autophagy influx and not due to impedance of autophagosome maturation.

This increase in LC3-II protein might be also due to transcriptional upregulation of *Maplc3b* encoding a major form of LC3. By quantitative real-time PCR of *Maplc3b*, we observed that the transcriptional level of LC3 was significantly higher in *Lmna*$^{H222P/H222P}$ compared with wild-type MEF (Fig. 6B, $p = 0.0141$); relative copy number of LC3 mRNA in *Lmna*$^{H222P/H222P}$ MEF was 1.36 times when standardized by G3PDH transcriptional level.

Inhibition of autophagy increased the frequency of nuclear abnormalities and decreased cell viability in *Lmna*$^{H222P/H222P}$ MEF. To elucidate the role of autophagy in *Lmna*$^{H222P/H222P}$ cells, we inhibited autophagy by using 3-methyladenine (3-MA) and wortmannin. Autophagy was efficiently inhibited as the amount of LC3-II was notably decreased both in wild-type and *Lmna*$^{H222P/H222P}$ cells (Fig. 7A).

The number of LC3-positive autophagosomes was significantly decreased in the treated *Lmna*$^{H222P/H222P}$ cells compared with the untreated cells (Fig. 7B, $p < 0.0001$). Moreover, LC3 staining was

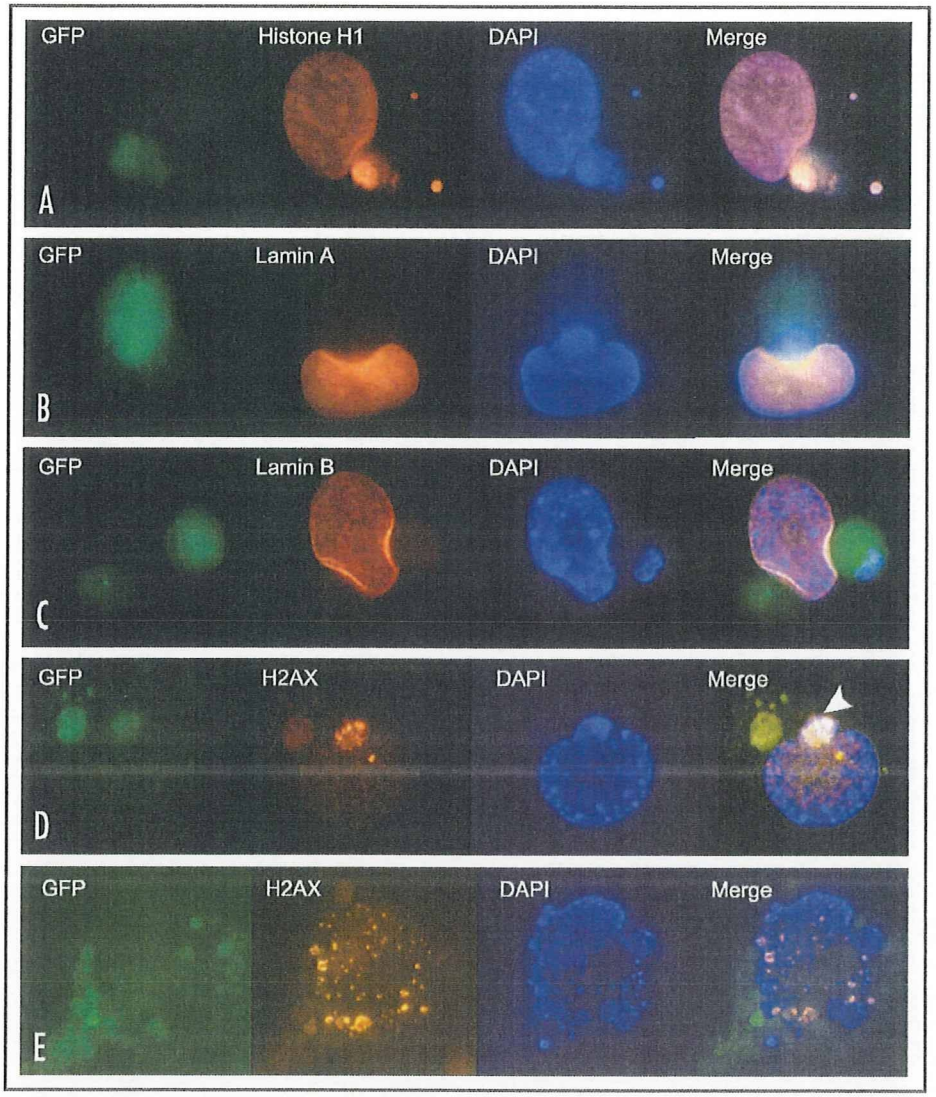

Figure 4. Involvement of autophagy-related proteins and LAMP2, and Lyso-Tracker® probe staining in *Lmna*$^{H222P/H222P}$/*GFP-LC3* MEF. Atg5 (A), Atg9 (B), Rab7 (C) and LAMP2 (D) are all remarkably stained in/around the GFP-positive structures. (E) Lyso-Tracker® is highlighted and localized with the GFP-positive structures near nucleus.

virtually absent in the treated cells, even in nuclei with markedly irregular shape and with extranuclear DAPI signals, whereas it was often presented in untreated cells (Fig. 7C, upper). In addition, the number of cells with markedly irregular nuclei and/or extranuclear DAPI, as represented in Figure 7C, was much increased when autophagy was inhibited: the percentage of cells with nuclear deformation was 6.7 ± 1.2 and 9.8 ± 1.6 (mean ± SD), and cells with single or multiple extranuclear DAPI was 8.3 ± 0.9 and 14.9 ± 1.5 in untreated and treated cells, respectively (Fig. 7D). The difference between the two groups was statistically significant ($p = 0.0008$) after treatment.

We also checked mean survival rate by staining viable and dead cells in untreated wild-type (0.88), treated wild-type (0.83), untreated *Lmna*$^{H222P/H222P}$ (0.87) and treated *Lmna*$^{H222P/H222P}$ (0.72) cells (Fig. 7E). When autophagy was inhibited, the survival rate of *Lmna*$^{H222P/H222P}$ cells was significant decreased ($p = 0.0029$) as compared to wild-type cells. This result implies that autophagy could have a beneficial effect on cell survival.

Discussion

Here we provide evidence that a part of the nucleus is degraded by autophagy when nuclei are damaged and/or partially extruded into the cytoplasm as frequently observed in nuclear envelopathy.

In *Lmna*$^{H222P/H222P}$/*GFP-LC3* MEF, GFP-positive signals were presented near nuclei, which were proved to be identical to LC3-positive autophagosomes. The difference in staining

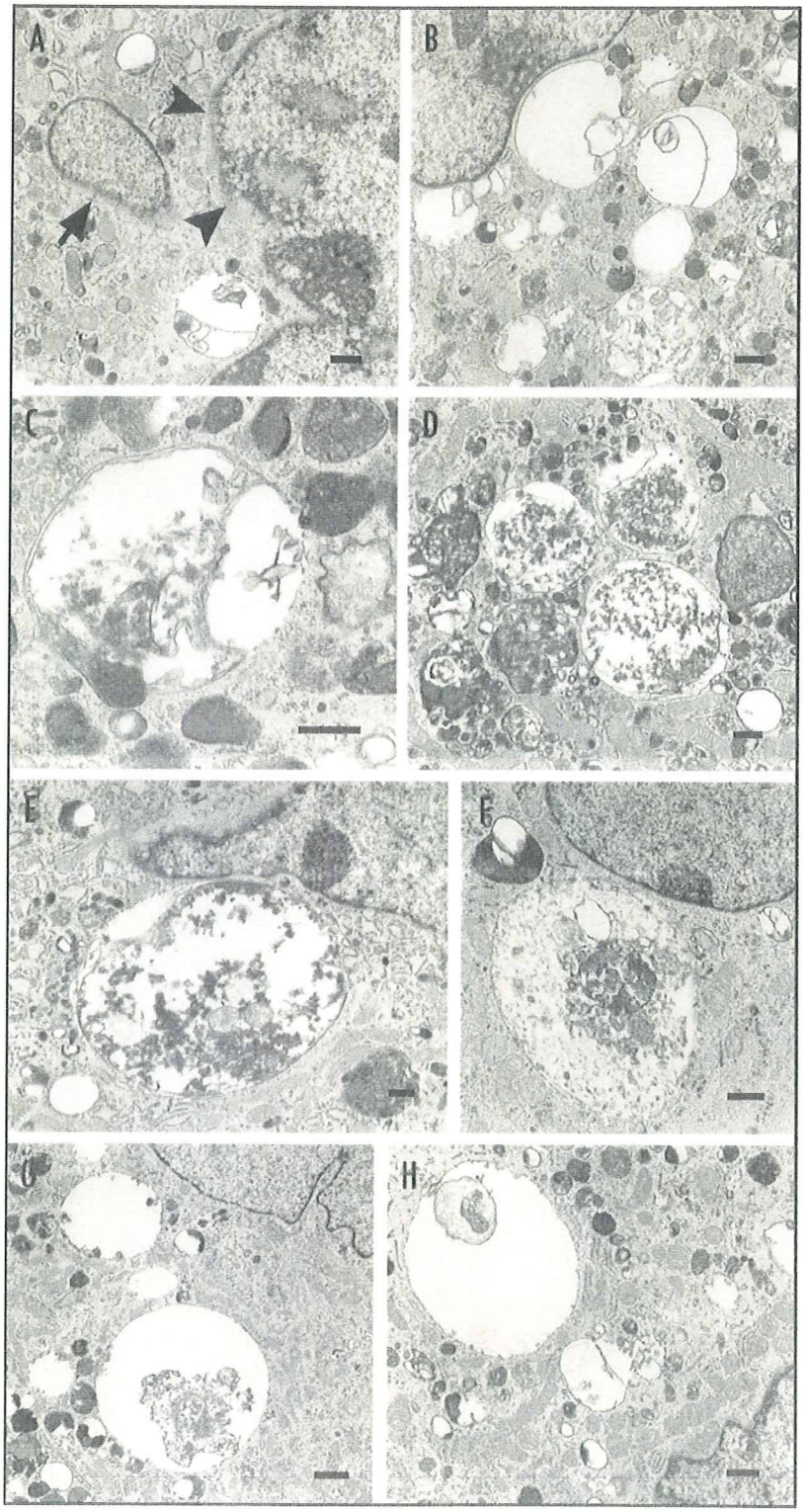

Figure 5. Characterization of nuclear components contained in the GFP-positive autophagosomes on immunocytochemistry. (A–C) GFP-positive autophagosomes with variable sized are seen close to the nuclei, and most of which are partially colocalized with DAPI signals outside of nucleus. Extranuclear DAPI signals in the GFP-positive autophagosomes are positive for histone H1 (A), but not for nuclear envelope proteins such as lamin A and B (B and C). (D) Extranuclear DAPI signals with GFP staining are positive for γH2AX (arrowhead). (E) Nuclear fragments with scattered γH2AX staining are negative for LC3.

pattern between GFP and LC3 despite their essential identity is probably due to the accumulation of GFP that is resistant to lysosomal hydrolase. Further immunostaining of other autophagy-related proteins (i.e., Atg5, 16L, 9 and Rab7) and LAMP2 confirmed that the GFP-positive signals are ultimately autophagosomes and autolysosomes. Our findings indicate that the autophagosomes appear to degrade the extruded nuclear components since most of them contained extranuclear DAPI and major histone protein H1 within. Irregularly blurred or faint DAPI or H1 signals inside the autophagosomes/autolysosomes substantiate that nuclear components are being degraded by autophagic process. The target of autophagy is probably the damaged portions of nuclei as demonstrated by γH2AX immunostaining.

Electron microscopic observations of $Lmna^{H222P/H222P}$ cells demonstrated that autophagosomes were clustered and lysosomes fused to form giant autophagosomes, which were sometimes bigger than nuclei. Giant autophagosomes are quite unusual and are rarely seen in starvation-induced autophagy, where the size is about 1 μm.[35] Similar large-sized (5 to 10 μm) autophagosomes has been reported to encircle bacteria in HeLa cells under group A streptococcus infection although the mechanism to form such giant autophagosomes was not clarified.[41] From our findings it can be suggested that the formation of giant autophagosomes may be required for the degradation of large molecules, such as a part of nucleus.

We propose that $Lmna^{H222P/H222P}$ nuclei, having incomplete lamina structure and frequently subjected to mechanical stress, subsequently become damaged and would apparently require (giant) autophagosome for degradation by lysosomal enzymes. Thus, it seems that this nuclear autophagy is consistent with macroautophagy in terms of its morphology and machinery used. On the other hand, piecemeal microautophagy of nucleus (PMN) has been recently